



Office of Research, Development, Test, and Evaluation

# Stockpile Stewardship Quarterly

VOLUME 4

| NUMBER 4

| DECEMBER 2014

## Message from the Assistant Deputy Administrator for Research, Development, Test, and Evaluation, Dr. Kathleen Alexander

The Research, Development, Test, and Evaluation (RDT&E) team has had an extremely successful year—our experimental facilities are producing data in new regimes with record efficiencies and throughput. Our modeling and simulation capabilities are improving and the resultant analysis is contributing directly to stockpile stewardship efforts. We have much to be proud of as a team, and I look forward to our successes in the coming year.

This issue of *Stockpile Stewardship Quarterly* highlights some of the experiments and modeling which support the Stockpile Stewardship Program. These span a range in the RDT&E portfolio from high energy density experiments and modeling without high explosives (HE) to HE experiments with additives to electrical circuits in hostile environments.

Our first technical article by Malcolm Andrews describes the latest modeling of weapon physics experiments which involve ejected materials. This research provides for the first time a predictive framework for ejecta experiments. The next article by J. Tiberius Morán-López studies turbulent mixing due to the Richtmyer-Meshkov instability in a broad range of experiments of interest to stockpile stewardship.

The article by Wagner, Beresh, and Kearney discusses how metal particles are often added to explosives to alter



Dr. Kathleen Alexander with (left to right) Dr. Richard Petrasso, head of the High-Energy-Density Physics Division of the Massachusetts Institute of Technology (MIT) Plasma Science and Fusion Center; Dr. Mario Manuel, the 2014 recipient of the Marshall Rosenbluth Outstanding Thesis Award presented by the American Physical Society (see page 6), and Dr. Don Cook, Deputy Administrator for Defense Programs. Both Drs. Cook and Manuel received their PhDs from the MIT Nuclear Science and Engineering Department.

performance. The complex trajectories and speeds of densely packed particles in metalized explosives are studied using the Multiphase Shock Tube at Sandia National Laboratories. The next article by Prestridge, Charonko, and Garcia highlights Los Alamos National Laboratory's study of variable density mixing using multi-phase shock tube experiments. For the first time, high resolution measurements of shock-driven variable-density flows are studied in support of code validation. The final article in this issue by Hembre and Keiter describes the precision modeling of electrical circuits in hostile environments. Some of these issues are also of interest to the electronics industry.

We highlight the achievements of two students—Mario Manuel (pictured) won the prestigious Rosenbluth award for his outstanding thesis “Rayleigh-Taylor-Induced Electromagnetic Fields in Laser-Produced Plasmas” at MIT. This was the first Rosenbluth award in high energy density/inertial confinement fusion physics. Mike Rosenberg defended his thesis supported by the National Ignition Facility (NIF) PhD Thesis Program, which is now the second thesis based on NIF data (see page 6). The NIF data he used focused on exploding pusher shots of deuterium-helium-3 and deuterium-deuterium filled capsules.



### Inside

- 2 Recent Progress with Ejecta Modeling at Los Alamos National Laboratory
- 3 Modeling the Effects of Hydrodynamic Instability-Induced Turbulent Mixing for Low-to-Moderate Shock Mach Numbers
- 7 Developing a Predictive Capability for Explosive Phenomena Using a Multiphase Shock Tube
- 9 The Los Alamos National Laboratory Turbulent Mixing Tunnel
- 11 Precision Calculations for Circuits in Hostile Environments

### Comments

The *Stockpile Stewardship Quarterly* is produced by the NNSA Office of Research, Development, Test, and Evaluation. Questions and comments regarding this publication should be directed to Terri Stone at [terri.stone@nnsa.doe.gov](mailto:terri.stone@nnsa.doe.gov). | Technical Editor: Dr. Joseph Kindel | Publication Editor: Millicent Mischo

## Recent Progress with Ejecta Modeling at Los Alamos National Laboratory by Malcolm J. Andrews (Los Alamos National Laboratory)

The term *ejecta* refers to the removal of mass from a material surface due to the passage of a shock through that surface, its subsequent movement through a participating medium, and its ultimate conversion (perhaps recollection or evaporation). At Los Alamos National Laboratory (LANL), these three distinct steps are respectively referred to as source, transport, and conversion. Driven materials are well known to produce a spread of mass scooped out as a shock passes through the surface, and can form a jet of small particles. Thus, this article concerns itself with mathematical models that describe this ejecta process of distributing mass from a surface to a surrounding volume.

There have been numerous experiments that have sought to characterize ejecta, particularly the source, as transport and conversion are often thought of as being of lesser importance. Until about five years ago, the approach to understand ejecta sources focused on experimental characterization, which was then parameterized and used for predictive simulations. Such an approach was first developed and used by Lawrence Livermore National Laboratory (LLNL), with the United Kingdom's Atomic Weapons Establishment (AWE) shortly thereafter. This encompassing approach took ejecta experiments that spanned a 20-year period and produced a useful correlation technique.

At that time, LANL had no dynamic ejecta model, but recognized the advance and coherency in the LLNL approach. To develop a more predictive model, LANL has taken a different route, using the fact that the ejecta phenomena originate from a Richtmyer-Meshkov instability (RMI) that occurs as a shock passes through the crinkled interface between two different density materials. However, for ejecta the typical Atwood number

$$(A_t \equiv (\rho_{heavy} - \rho_{light}) / (\rho_{heavy} + \rho_{light})),$$

a non-dimensional density ratio, is close to 1, and special theories were needed. Fortunately, Mikaelian at LLNL had been developing just such theories based on original Richtmyer work, and on Layzer research for Rayleigh-Taylor (the RMI equivalent for steadily driven

instabilities). With that foundation, Buttler<sup>1</sup> and Dimonte<sup>2</sup> developed RMI-based mathematical models for sources of ejecta from liquid/vacuum, liquid/gas, and solid/gas configurations. The vacuum case is the focus here as there is an extensive set of data from Buttler,<sup>1,3</sup> whose experiments

were supported by the Science Campaign at LANL. Moreover, in a vacuum the Atwood number is exactly 1 and thus measurements of mass released are due solely to the shock passage and RMI, so that downstream measurements are not convolved with the participating material. This thought is consistent with the source concept for the overall ejecta description given above, and means that we can perform independent source and transport experiments, and thus separate the physical processes. An added complexity that can occur in applications is a second shock interaction with the surface, that might occur sometime after the first shock has passed. The difficulty with the second shock is that the surface will have already sourced ejecta and thus the surface may not be well characterized, leaving poorly defined initial conditions.

The following briefly describes the first and second shock ejecta source models that LANL has developed and implemented in its Advanced Simulation and Computing code. Transport and conversion models will be discussed in a future article.

Details of the mathematical development of the LANL ejecta model are left to the references and instead the key results from Buttler<sup>1</sup> are quoted (the Dimonte<sup>2</sup>

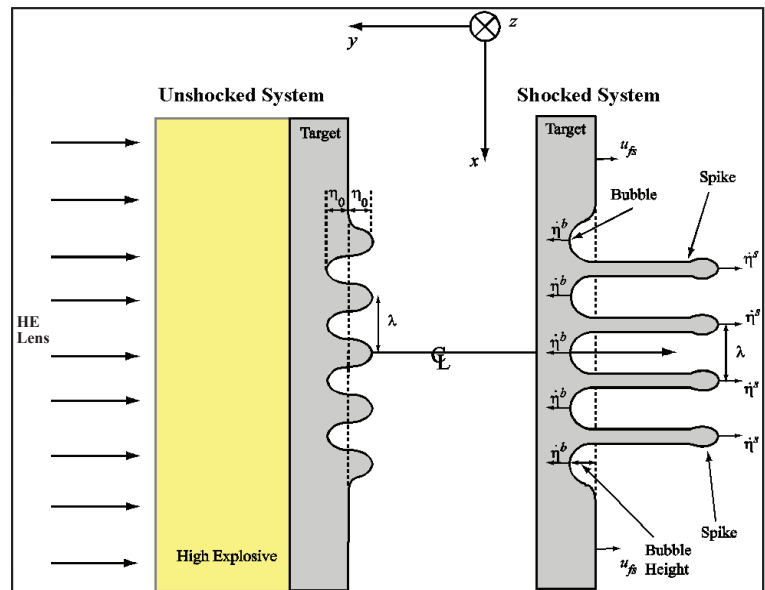


Figure 1. RMI evolution of bubbles and spikes for ejecta source.

model is in the same RMI family). The surface of the liquid metal is envisaged in Figure 1, and may be conveniently described as the shock driving bubbles to excavate material mass out from the surface and into the spikes. The theory produces two key parameters, namely the bubble tip velocity,  $\dot{\eta}^b$ , and the spike tip velocity,  $\dot{\eta}^s$ ; formulas for these parameters can be summarized as:

Equation 1

$$\dot{\eta}^b(t) = \frac{\dot{\eta}_0^b}{1 + \frac{3}{2} \dot{\eta}_0^b k t}, \text{ and } \dot{\eta}_0^s \approx \sqrt{3} \dot{\eta}_0^b \quad (1)$$

The subscript "0" refers to initial time values (i.e., immediately after the shock has passed), and wavenumber  $k$  ( $\equiv 2\pi/\lambda$ ) where  $\lambda$  is the wavelength of the initial perturbation. Of particular interest in Equation 1 for the bubble (left) is to note the inverse time decay of the bubble velocity, and that shorter wavelengths (higher wavenumbers) decay faster. In contrast, the spike attains a steady terminal velocity. The difference lies in the low drag and added mass of the spike compared with the bubble, which causes the bubble to slow inversely with time. The areal mass (mass per unit area) excavated and then ejected by the bubble is readily computed from Equation 1 as:

Equation 2

$$m/A = \int_0^t \dot{\eta}^b(\omega) S_f d\omega = m_0 \ln(1+t/\tau) \quad (2)$$

where  $S_f$  is a shape factor that is taken as 1 for convenience,  $m_0 = \rho\lambda/3\pi$ , and  $\tau = \lambda/(3\pi\dot{\eta}_0^b)$ . Thus, Equation 2 is the basic ejecta source model and has been successfully validated experimentally by Buttler.

How then does one mathematically describe ejecta formation from second shock? The fundamental problem is to know what the surface profile might look like at second shock, a difficult problem for which no experimental data has been collected. The LANL approach has been to state a hypothesis for the surface condition at second shock, and then explore its validity. The hypothesis is: "It is the longest wavelength and its amplitude on the surface of the material that determine most of the mass source." The hypothesis is motivated by the observation above that short wavelength (high wavenumber) perturbations decay quickly (see Equation 1), and leave longer wavelengths to excavate most of the mass (see Equation 2). One immediate consequence is that shapes with similar wavelengths and amplitudes will source similar areal masses. A demonstration of this effect can be seen in Figure 2 where numerical simulations that used initial Sine, Chevron and Fly-Cut shapes produce similar bubble and jet configurations. The resulting areal masses are plotted in Figure 3 and are practically the same. Indeed, closer

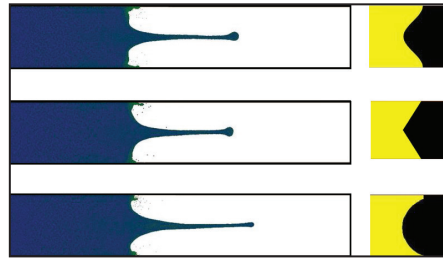


Figure 2. Initial surface profiles (Sine, Chevron, Fly-Cut) and late-time Spike/Bubble Evolution.

inspection of Figure 2 reveals that the bubbles have evolved from the Sine to the Fly-Cut shape. This evidence, and much more presented in a 2013 report, has verified the hypothesis and led to the following model for second shock ejecta: the amplitude of the surface bubble perturbations as they evolve after first shock are used as initial conditions at second shock, with the wavelength being that of the longest one used for the first shock source, and the amplitude taken as the bubble depth. It is the recognition that bubble shape evolution does not significantly affect the source that makes the hypothesis effective. Moreover, in principle, the argument for second shock applies to subsequent shocks and thus, provides a more general framework, but this remains to be established.

Our progress with first and second shock models of ejecta is fueling our interest to explore the validity for the hypothesis for more complex shapes. Moreover, we also seek to extend the model to solid surfaces (i.e., to handle strength). Much

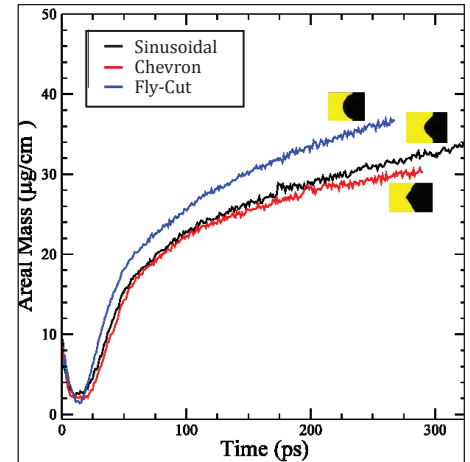


Figure 3. Ejected areal mass ( $M/A$ ) from different initial grooves.

still remains to be done, but our liquid ejecta first and second shock models provide, for the first time, a complete predictive framework for ejecta source that can be further validated against experiment, and form a basis for future extensions and improvements.

## References

- W.T. Buttler, D.M. Oro, D.L. Preston, K.O. Mikaelian, F.J. Cgerne, R.S. Hixson, F.G. Mariam, C. Morris, J.B. Stone, G. Terrones, and D. Tupa, "Unstable Richtmyer-Meshkov Growth of Solid and Liquid Metals in Vacuum," *J. Fluid Mech.* 703, 60-84, 2012.
- G. Dimonte, G. Terrones, F.J. Cherne, and P. Ramaprabhu, "Ejecta Source Model Based on the Nonlinear Richtmyer-Meshkov Instability," *J. Appl. Phys.* 113, 024905, 2013.
- Mark Anderson, "Developing a Predictive Capability," *Stockpile Stewardship Quarterly* 4, 1, pp. 6-7, March 2014. •

## Modeling the Effects of Hydrodynamic Instability-Induced Turbulent Mixing for Low-to-Moderate Shock Mach Numbers by J. Tiberius Morán-López (National Nuclear Security Administration)

### Introduction and Motivation

The effects of multi-fluid hydrodynamic instabilities and turbulent mixing are ubiquitous and manifested in many familiar situations. Turbulence is present in geophysical flows such as rivers and oceans, where density fluctuations develop due to temperature and salinity effects. The mixing of cream in coffee and smoke rising from a cigarette show transitions from laminar to turbulent flows.<sup>1</sup> Unsteady flows are also common in aviation, as atmospheric flows are

susceptible to strong turbulence. In science and engineering, the generation and evolution of turbulence from variable-density and compressible hydrodynamic instabilities are often critically important.<sup>2</sup> Many applications in gas dynamics typically have large Reynolds numbers (i.e., the ratio of inertial to viscous forces) and are, therefore, turbulent.<sup>3</sup> Other applications ranging from the transonic to supersonic regimes include high-speed flight and supersonic combustion ramjet engines.<sup>4</sup>

Similarly, turbulent mixing can significantly impact high energy density (HED) systems,<sup>5,6</sup> which encompass astrophysical phenomena, inertial confinement fusion (ICF), high-energy laser and shock tube experiments, and laboratory astrophysics investigations—all of which are relevant to stockpile stewardship science. Moreover, these problems increase in complexity as shocks and blast waves are also generated from large and instantaneous releases of energy. In supernovae dynamics, ionizing radiation and

turbulence from blast and shock wave instabilities<sup>7</sup> are critical to stellar and galaxy formation; molecular clouds in the interstellar medium (ISM) are strong sources of ionizing radiation and turbulence capable of supporting gravitational collapse, thus sustaining star formation.<sup>8</sup> Thermonuclear fuel compression in ICF is highly susceptible to shock-induced hydrodynamic instabilities, where instabilities leading to turbulent mixing limit thermonuclear fuel compression and ignition by mixing ablative shell material with the deuterium-tritium fuel in the capsule.<sup>9,10</sup>

HED experiments have been successfully used to relate scaled models in controlled laboratory environments to astrophysical observations<sup>11</sup> and to probe hydrodynamic instability-induced turbulence.<sup>9</sup> In the past decades, experiments with various ICF capsule targets have demonstrated the important role of hydrodynamic instabilities and mixing in determining the efficiency of target implosion and the limiting of thermonuclear fuel compression.<sup>12</sup> However, generating astrophysical phenomena in the laboratory is challenging due to the high pressures and temperatures involved<sup>13</sup> and the complexity of scaling astrophysical scales to terrestrial scales.

Therefore, the development and demonstration of predictive methods are essential for conducting stockpile stewardship science. Numerical simulations and modeling can elucidate HED processes and instabilities, and provide guidance for experimental endeavors. Numerical codes can aid in exploring new ideas in a timely and efficient manner, as well as perform parametric studies that would be prohibitively expensive or unmanageable from an experimental approach. Thus, significant efforts have been dedicated to improve HED understanding through predictive modeling. This article summarizes recent modeling research that accurately predicts the evolution of reshocked Richtmyer–Meshkov instability (RMI) for numerous cases. Results are compared with experimental data, while numerical convergence under grid refinement is briefly discussed.

### An Overview of the Reshocked Richtmyer–Meshkov Instability

One instability that is prevalent in HED environments is the RMI,<sup>14,15</sup> which

occurs when an initially perturbed interface separating two fluids with different densities is impulsively accelerated by a shock (see Figure 1). This results in the amplification of interfacial perturbations and development of turbulent mixing at sufficiently large Reynolds numbers, amplifying shock and interface distortions.<sup>16,17</sup> In many applications, the evolving interface experiences multiple shock compressions from reflected shocks. Reshock occurs when one or more reflected shocks interact with the evolving mixing layer, resulting in enhanced turbulent mixing manifested by an amplified mixing layer growth rate (see Figure 2). The mixing layer develops as perturbations grow and lead to interpenetration of light fluid bubbles and heavy fluid spikes into the heavy and light gases, respectively.<sup>18,19</sup> The mixing layer growth can be measured experimentally and calculated from high-resolution numerical simulations to validate predictive models. It is important to understand the effects of reshocked RMI, as this instability is critical to many applications in HED science.

### A Brief Summary of Results

A weighted essentially nonoscillatory (WENO) shock-capturing method for solving the multicomponent Reynolds-averaged Navier–Stokes (RANS) equations using the  $K-\epsilon$  turbulence model<sup>21,22</sup> was used to model reshocked RMI. Moreover, the RANS model was independent of empirical calibrations (colloquially known as knobs), as a single coefficient set was used to predict the evolution of nine air/sulfur hexafluoride ( $\text{SF}_6$ ) reshocked RMI cases with  $A_t = 0.67$ . The Atwood number,  $A_t$ , is the difference in densities between the test section (driven) gas and the driver gas, divided by the sum of the densities. Positive and negative  $A_t$  values correspond to light-to-heavy and heavy-to-light initial gas transitions.

One factor impacting the time of reshock,  $\tau_R$ , is the test section length  $\delta$ , which

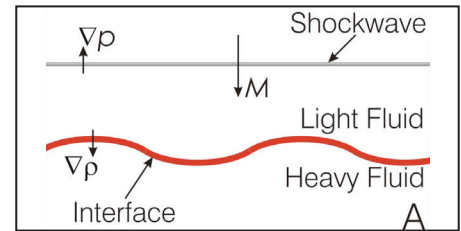


Figure 1. Schematic portraying shock-driven RMI.

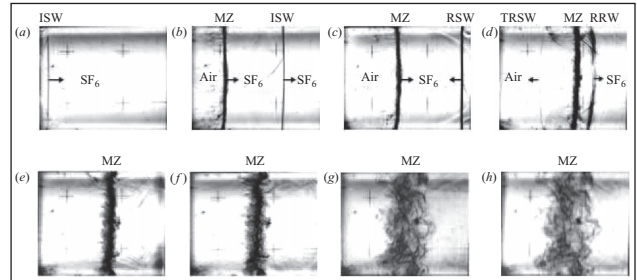


Figure 2. Progressive experimental images of reshocked RMI: incident shock accelerates interface; shock traveling ahead of interface, both propagate downstream; shock reflects from endwall, leading to reshock and enhanced turbulent mixing.<sup>20</sup>

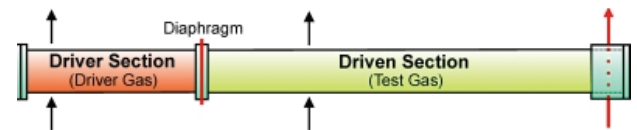


Figure 3. Shock tube with driver and test (driven) sections.

is the distance between the initial perturbed interface separating the two gases and the test section endwall (see Figure 3). As  $\delta$  increases, the shock traverses a greater distance and more time elapses before it reflects from the test section endwall and compresses the interface once again through reshock. Figure 4 presents RANS mixing layer predictions for shock Mach number  $Ma_s = 1.20$  with increasing test section length,  $8 < \delta < 23.5$  cm, to elucidate the corresponding increase in  $\tau_R$ . The data in Figure 4 compares RANS post-reshock growth rates  $h$  (proportional to the rate at which turbulent mixing is enhanced following reshock) with experimental data; tertiary data shows  $\tau_R$  correspondingly increasing with  $\delta$ .

A second factor affecting  $\tau_R$  and  $h$  is the shock strength. Hydrodynamic and turbulent pressures, shock speeds, and the turbulent Mach number increase as  $Ma_s$  grows. As a result, contributions from larger pressure, velocity, and density gradients during

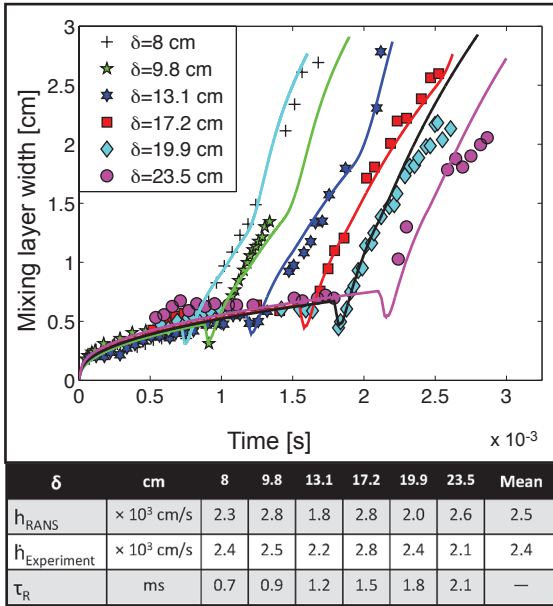


Figure 4. RANS predictions and experimental data<sup>20</sup> for  $A_t=0.67$ ,  $Ma_s=1.20$  with  $8 \leq \delta \leq 23.5$  cm.<sup>18</sup>

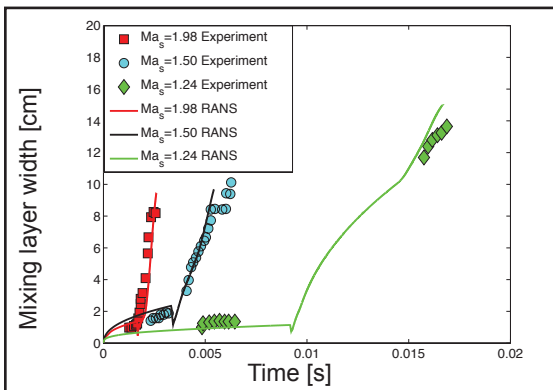


Figure 5. RANS predictions and experimental data<sup>14</sup> for  $A_t=0.67$ ,  $Ma_s=1.98, 1.50, 1.24$  with  $\delta=49, 61, 110$  cm, respectively.<sup>19</sup>

interface compression increase the rate at which turbulence is generated via buoyancy and shear production. Figure 5 compares RANS predictions with three  $A_t = 0.67$  experiments with increasing shock strength:  $Ma_s = 1.24, 1.50, 1.98$  with  $\delta = 110, 62, 49$  cm, respectively. This plot illustrates larger reshocks and post-reshock growth rates as the relative amount enhanced with increasing  $Ma_s$ .

Previous experiments<sup>16,17,20,23,24</sup> and numerical simulations<sup>25-32</sup> have shown that reshock significantly increases the mixing layer growth rate, enhancing turbulent mixing. The present RANS model further supports predictions consistent with these findings as it accurately predicts

the mixing layer widths for various  $A_t = 0.67$  experimental datasets. Moreover, numerical convergence is another critical component for establishing confidence in predictive methods. Unfortunately, this aspect is often overlooked as achieving convergence can be problematic in shocked flows due to shock, interface, and boundary discontinuities. Not presented here, convergence under grid refinement was also considered for mixing layer widths as well as for mean and turbulent fields for the nine cases presently discussed.

### Conclusions and Future Work

Simulations and modeling are critical for stockpile stewardship science. The further development of predictive simulation and modeling methods will help elucidate physical processes, as well as allow studies that are prohibitively expensive or perhaps not possible from an experimental perspective. Thus, significant efforts have been dedicated to understand, model, and predict HED processes with higher accuracy and fidelity.

This study briefly presented and discussed results accurately predicting turbulent mixing for reshocked RMI in HED environments using a newly developed WENO

implementation of the multicomponent RANS equations coupled with a  $K-\epsilon$  turbulence model. Mixing layer predictions were compared with experimental data for nine  $A_t = 0.67$  cases with  $1.20 < Ma_s < 1.98$  and  $8 < \delta < 110$  cm. Additional information on the model equations and coefficients, initial conditions, numerical implementation, numerical convergence, systematic studies, and comparisons to other predictive methods can be found in references 21, 22, and 33.

With the goal of advancing predictive capabilities for stockpile stewardship science, significant efforts have been dedicated to improve current modeling and simulation capabilities. The present

RANS model is being further developed to achieve higher accuracy, improve the convergence rate, and cover a broader spectrum of applicability. Improvements will extend the ability of the model to simulate reshocked RMI for larger shock Mach numbers ( $2 < Ma_s < 5$ ), as well as predicting a broader spectrum of light-to-heavy and heavy-to-light transitions using other gas pairs (e.g., H, He, Ar,  $CO_2$ , Kr). As further confidence is established in the model, the incorporation of additional HED-relevant physics is planned.

### References

- R.P. Drake, "High-Energy-Density Physics: Fundamentals, Inertial Fusion, and Experimental Astrophysics," Springer-Verlag, 2006.
- P. Chassaing, R.A. Antonia, F. Anselmetti et al. "Variable Density Fluid Turbulence," Fluid Mechanics and Its Applications Vol. 69, Kluwer Academic, 2002.
- L.D. Landau and E.M. Lifshitz, Fluid Mechanics: Course of Theoretical Physics Vol. 6, Elsevier, 1987.
- C. Segal, The Scramjet Engine: Processes and Characteristics, Cambridge Aerospace Series No. 25, Cambridge Univ. Press, 2009.
- Y. Zhou et al., "Progress in Understanding Turbulent Mixing Induced by Rayleigh-Taylor and Richtmyer-Meshkov Instabilities," Phys. Plasmas 10, 1883-1886, 2003.
- J. Colvin and J. Larsen, Extreme Physics: Properties and Behavior of Matter at Extreme Conditions, Cambridge University Press, 2013.
- J. Grun, J. Stamper, and C. Manka et al., "Instability of Taylor-Sedov Blast Waves Propagating Through a Uniform Gas," Phys. Rev. Lett. 66, 2738-2741, 1991.
- T. Gritschneder, T. Naab, S. Walch et al., "Driving Turbulence and Triggering Star Formation by Ionizing Radiation," Astrophys. J. 694, L26-L30, 2009.
- O.A. Hurricane, V.A. Smalyuk, K. Raman et al., "Validation of a Turbulent Kelvin-Helmholtz Shear Layer Model Using a High-energy-density OMEGA Laser Experiment," Phys. Rev. Lett. 109, 155004, 2012.
- J.D. Lindl, Inertial Confinement Fusion: The Quest for Ignition and Energy Gain Using Indirect Drive, AIP Press, 1998.
- C.C. Kuranz et al., "Progress Toward the Study of Laboratory Scale, Astrophysically Relevant, Turbulent Plasmas," Astrophys. Space Sci. 298, 9-16, 2004.
- S. Atzeni and J. Meyer-ter-Vehn, The Physics of Inertial Fusion: Beam Plasma Interaction, Hydrodynamics, Hot Dense Matter, Internat. Series of Monographs on Physics Vol. 125, Oxford Univ. Press, 2004.

<sup>13</sup>A.B. Reighard, "Collapsing Radiative Shock Experiments on the Omega Laser, PhD dissertation, University of Michigan, 2007.

<sup>14</sup>R.D. Richtmyer, "Taylor Instability in Shock Acceleration of Compressible Fluid," *Comm. Pure Appl. Math.* 13, 297-319, 1960.

<sup>15</sup>E.E. Meshkov, "Instability of the Interface of Two Gases Accelerated by a Shock Wave," *Sov. Fluid Dyn.* 4, 101-108, 1969.

<sup>16</sup>M. Vetter and B. Sturtevant, "Experiments on the Richtmyer-Meshkov Instability of an Air/SF<sub>6</sub> Interface," *Shock Waves* 4, 247-252, 1995.

<sup>17</sup>F. Poggi et al., "Velocity Measurements in Turbulent Gaseous Mixtures Induced by Richtmyer-Meshkov Instability," *Phys. Fluids* 10, 2698-2700, 1998.

<sup>18</sup>M. Brouillette, "The Richtmyer-Meshkov Instability," *Annu. Rev. Fluid Mech.* 34, 445-468, 2002.

<sup>19</sup>O. Schilling and J.W. Jacobs, "Richtmyer-Meshkov Instability and Re-accelerated Inhomogeneous Flows," *Scholarpedia* 3, 6090, 2008.

<sup>20</sup>E. Leinov et al., "Experimental and Numerical Investigation of the Richtmyer-Meshkov Instability Under Re-shock Conditions," *J. Fluid Mech.* 626, 449-475, 2009.

<sup>21</sup>J.T. Morán-López and O. Schilling, "Multi-component Reynolds-averaged Navier-Stokes Simulations of Richtmyer-Meshkov

Instability and Mixing Induced by Reshock at Different Times," *Shock Waves* 24, 325-343, 2014.

<sup>22</sup>J.T. Morán-López and O. Schilling, "Multi-component Reynolds-averaged Navier-Stokes Simulations of Reshocked Richtmyer-Meshkov Instability-induced Mixing," *High Energy Dens. Phys.* 9, 112-121, 2013.

<sup>23</sup>B.J. Balakumar et al., "Turbulent Mixing in a Richtmyer-Meshkov Fluid Layer After Reshock: Velocity and Density Statistics," *J. Fluid Mech.* 696, 67-93, 2012.

<sup>24</sup>C. Weber et al., "Richtmyer-Meshkov Instability on a Low Atwood Number Interface After Reshock," *Shock Waves* 22, 317-325, 2012.

<sup>25</sup>D.J. Hill, C. Pantano, and D.I. Pullin, "Large-eddy Simulation and Multiscale Modeling of a Richtmyer-Meshkov Instability with Reshock," *J. Fluid Mech.* 557, 29-61, 2006.

<sup>26</sup>M. Latini, O. Schilling, and W.S. Don, "Effects of WENO Flux Reconstruction Order and Spatial Resolution on Reshocked Two-dimensional Richtmyer-Meshkov Instability," *J. Comput. Phys.* 221, 805-836, 2007.

<sup>27</sup>O. Schilling, M. Latini, and W.S. Don, "Physics of Reshock and Mixing in Single-mode Richtmyer-Meshkov Instability," *Phys. Rev. E* 76, 026319, 2007; Erratum, *Phys. Rev. E* 85, 049904, 2012.

<sup>28</sup>O. Schilling and M. Latini, "High-order WENO Simulations of Three-dimensional

Reshocked Richtmyer-Meshkov Instability to Late Times: Dynamics, Dependence on Initial Conditions, and Comparisons to Experimental Data," *Acta Mech. Scientia* 30B, 595-620, 2010.

<sup>29</sup>F.F. Grinstein, A.A. Gowardhan, and A.J. Wachtor, "Simulations of Richtmyer-Meshkov Instabilities in Planar Shock-tube Experiments," *Phys. Fluids* 23, 034106, 2011.

<sup>30</sup>M. Hahn, D. Drikakis, D.L. Youngs, and R.J.R. Williams, "Richtmyer-Meshkov Turbulent Mixing Arising from an Inclined Material Interface with Realistic Surface Perturbations and Reshocked Flow," *Phys. Fluids* 23, 046101, 2011.

<sup>31</sup>B. Thornber, D. Drikakis, D.L. Youngs, and R.J.R. Williams, "Growth of a Richtmyer-Meshkov Turbulent Layer After Reshock," *Phys. Fluids* 23, 095107, 2011.

<sup>32</sup>B.D. Collins and J.W. Jacobs, "PLIF Flow Visualization and Measurements of the Richtmyer-Meshkov Instability of an Air/SF<sub>6</sub> Interface," *J. Fluid Mech.* 464, 113-136, 2002.

<sup>33</sup>J.T. Morán-López, "Multicomponent Reynolds-Averaged Navier-Stokes Modeling of Reshocked Richtmyer-Meshkov Instability-Induced Turbulent Mixing Using the Weighted Essentially Nonoscillatory Method," PhD dissertation, University of Michigan, Ann Arbor, 2013. •

## Highlights

### Rosenbluth Award Recipient

**Mario J. Manuel**, recent Massachusetts Institute of Technology PhD in Applied Plasma Physics (2013) from the Nuclear Science and Engineering Department, is the latest Marshall Rosenbluth Outstanding Thesis Award recipient, and the first ever from the field of high energy density/inertial confinement fusion physics. Dr. Manuel received the prestigious award in October for his thesis "Rayleigh-Taylor-Induced Electromagnetic Fields in Laser-Produced Plasmas" through the High Energy Density Division, led by Dr. Richard D. Petrasso of the Plasma Science and Fusion Center. Dr. Manuel's dissertation research focused on the development of a monoenergetic proton radiography system to make the first experimental measurements of magnetic fields induced by Rayleigh-Taylor growth in laser-produced plasmas and derives entirely out of the National Laser Users' Facility Program. Established in 1985 as the Simon Ramo Award

(later the Outstanding Doctoral Thesis in Plasma Physics Award), the award recognizes exceptional young scientists who have performed original doctoral thesis research of outstanding scientific quality and achievement in the area of plasma physics. •

### National Ignition Facility (NIF) PhD Thesis Program

Massachusetts Institute of Technology (MIT) graduate student **Mike Rosenberg** recently defended his thesis as part of the NIF PhD Thesis Program. His is now the second thesis based on NIF data, with two more NIF-based theses occurring this spring. Rosenberg's advisor is Dr. Richard Petrasso, who heads the High Energy Density Physics Division at MIT's Plasma Science and Fusion Center.

The NIF data he used focused on exploding pusher shots of deuterium-helium-3 (D<sup>3</sup>He) and deuterium-deuterium-filled capsules for studies of kinetic and multi-ion effects. While the shots were primarily for diagnostic development, he was able to use them



for physics research. An important finding of his research was that the experimental yield from D<sup>3</sup>He exploding pushers is, for the limit of extreme kinetic-like implosions he studied, two orders of magnitude lower than predicted by average-ion radiation hydrodynamics codes. In contrast, for the very hydro-like exploding pusher implosions, Rosenberg found that the average-ion radiation hydrodynamic codes accurately predicted yields and all other important implosion parameters. These results also bear upon the NIF ignition implosions since, during the shock convergence phase, the implosion is very kinetic-like before evolving into a very hydro-like phase. Another critically important consequence of Rosenberg's work is that it has formed the basis of the development of the NIF D<sup>3</sup>He monoenergetic proton backlighter platform for NIF Discovery Science. The first such shot will occur in March 2015. This work was accepted for publication in *Physics of Plasmas* under the title "Investigation of Ion Kinetic Effects in Direct-Drive Exploding-Pusher Implosions at the NIF." The tentative publication date is January 2015. •

## Developing a Predictive Capability for Explosive Phenomena Using a Multiphase Shock Tube

by Justin L. Wagner, Steven J. Beresh, and Sean P. Kearney (Sandia National Laboratories)

The Sandia National Laboratories (SNL) multiphase shock tube (MST) was constructed in 2010 to provide experimental data for metalized explosive detonation involving densely packed particles. Metal particles are often added to conventional high explosives to modify their performance.<sup>1</sup> In the early stages of a metalized explosive detonation, densely packed particles are dispersed by the high-speed expanding gas products. Since these particles are an integral part of the explosive event, the dynamics of their dispersion are critical to the continuing explosive reaction. Developing predictive capabilities for metalized explosives, therefore, requires detailed physical knowledge of how densely packed particles move in a high-speed gas. If predictions cannot correctly simulate these early stages of an explosion, they will fail at the later stages as well.

Until recently, however, a lack of experimental data precluded such a physical understanding. The effective drag of the densely distributed particles must be determined to correctly model the trajectories and speeds of the explosive particles.<sup>2</sup> Many engineering textbooks contain drag curves for a single particle, but the drag of densely packed particles behaves quite differently and does not have robust predictions. To remedy this, SNL's MST (see Figure 1) was constructed.

Like any standard shock tube, the MST includes a high pressure "driver" section and a low pressure "driven" section, which are initially separated by a diaphragm. The shock tube is initiated by rupturing the diaphragm, which creates a shock wave that propagates down the length of the tube through the driven section. A high speed gas flow follows the shock wave and provides a testing environment that can be used to study particle dynamics, which typically lasts only a few milliseconds.

Shock tubes have been utilized for over 100 years, but the MST is unique thanks to its ability to introduce a dense distribution of particles into its test section.<sup>3</sup> This is done with a gravity-fed apparatus that essentially amounts

to a hopper. A gate valve separates the hopper and shock tube. When the gate valve is opened, particles flow through an insert in the MST's ceiling, shaping them into the "particle curtain" also seen in Figure 1. In this case, the particles are inert glass spheres having a diameter of approximately 100 microns. The particle curtain has a thickness of about 2 mm in the flow direction. Most importantly, the fraction of volume occupied by particles in the curtain is about 20%, which places it in a dense regime relevant to explosives. Reliable drag curves are not available for this regime. Once the particle curtain is formed, the shock tube's diaphragm bursts and a shock wave travels towards the curtain. The curtain is then dispersed by the high-speed flow which follows the shock wave.

Images from a high-speed video captured during shock-induced particle dispersal are presented in Figure 2. The images were obtained using the Schlieren technique,<sup>4</sup> which is commonly used

in high-speed flow experiments. In its most basic form, the Schlieren method utilizes parallel light rays that are passed laterally through the shock tube's test section. When this light propagates through the test section, it refracts and bends as it traverses regions of varying gas density. This visualizes disturbances such as the shock waves shown in Figure 2. The dark region in the center of the images corresponds to the 2-mm-thick particle curtain, which appears in shadow where light cannot penetrate. In the left image, the shock is upstream of the curtain and seen as the black vertical line. The right image was obtained approximately 13 microseconds after the arrival of the shock at the curtain. As a result of an interaction of the shock wave with the particle curtain, a reflected shock and a transmitted shock are evident. The particles act as a porous medium with properties somewhere between a pure gas and a pure solid wall, creating the two shock waves. The particles are relatively large, however,

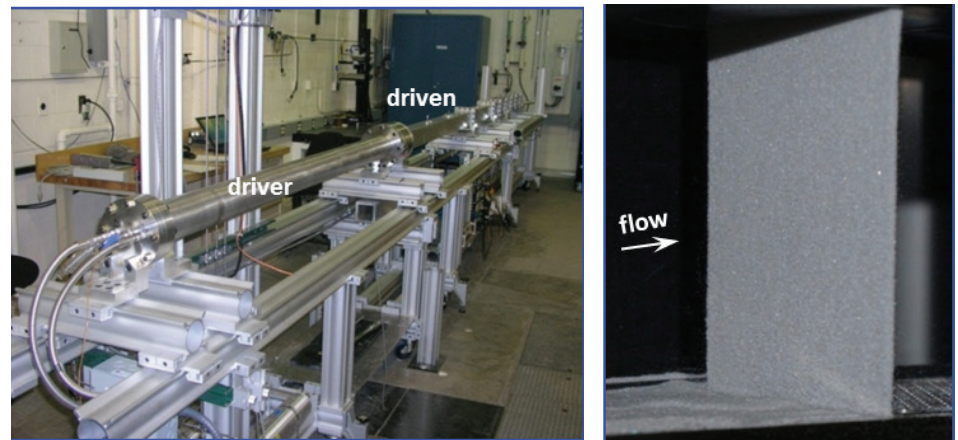


Figure 1. Multiphase shock tube (left) used to generate a dense particle curtain (right).

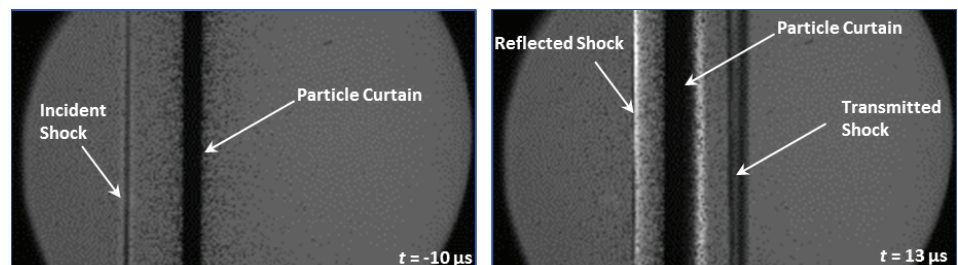


Figure 2. Images<sup>3</sup> showing the interaction of the initial shock wave with the particle curtain, before the arrival of the shock (left) and 13 microseconds after the shock impinges on the curtain (right).

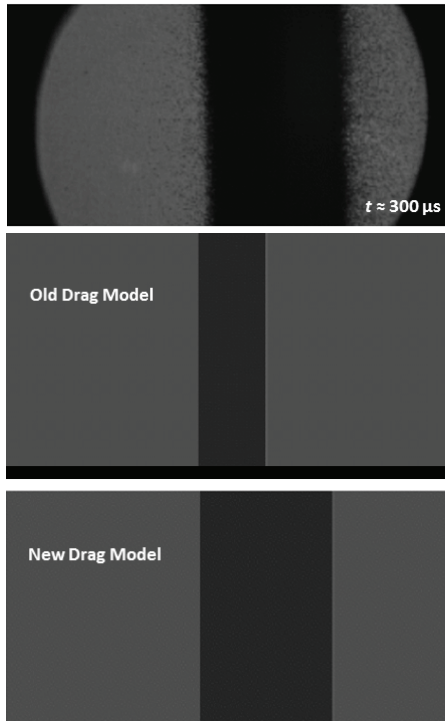


Figure 3. Experimental image showing particle dispersal approximately 300 microseconds after the arrival of the shock (top), simulated image using an old drag model (middle) and simulated image using a new drag model [Ling et al.] based on MST data (bottom).

and their inertia prevents them from moving much over the short time of 13 microseconds.

Obtaining particle dispersal data to develop better predictive models is precisely the purpose of the MST. An additional image, taken at a much later time of approximately 300 microseconds is shown in Figure 3. The particles in this image have had time to be accelerated by the high-speed gas flow surrounding them and, as a result, they moved substantially in comparison to their initial location. Moreover, the particle curtain has spread and now has a much greater thickness than its initial value. Though simplified, this particle dispersal process is analogous to that which occurs in explosive particle dispersal. The MST provides the experimental platform necessary to discover key physics and validation data to tune our predictive capabilities.

Comparisons of the experimental data to predictive models are also presented in Figure 3. The middle simulated image was obtained using a model based only on the drag of a single

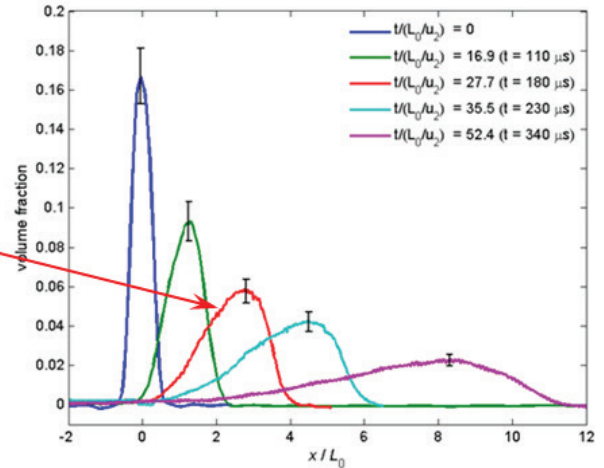
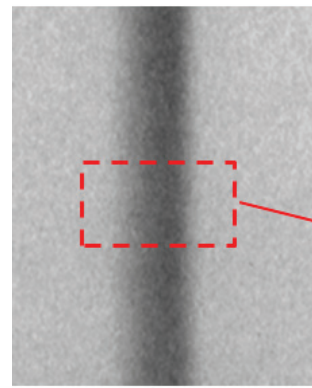


Figure 4. Radiograph of particle dispersal (left) and profiles of particle concentration obtained from the radiographs (right).

particle. Prior to the MST experiments, similar models were used in particle dispersal simulations. As the middle image shows, using this old model results in gross under-prediction of the particle movements. The bottom image was simulated using a new model incorporating the effects of densely distributed particles as revealed by the MST data.<sup>5</sup> In contrast, the new model does an excellent job of predicting the particle dispersal. This new model is currently being incorporated into predictive capabilities for explosive phenomena at SNL. Without MST data, our predictive capabilities for explosive particle dispersal would suffer.

Although our understanding of shock-induced particle dispersal has been improved over the last few years, additional data are required for model development. In particular, it is important to make measurements within the particle curtain, but it is opaque towards visible light and thus Schlieren imaging is no longer viable. X-rays, on the other hand, are able to penetrate the particle curtain. An example of an x-ray image obtained during shock-induced particle dispersal is shown in Figure 4. The image was obtained using a flash x-ray system, which outputs a high intensity burst of photons over a short time length of about 20 nanoseconds to capture a snapshot of the particle dispersal. The radiograph alone may not look impressive, but the intensity of the image can be converted to particle concentration to provide valuable quantitative information within the dense particle curtain.<sup>6</sup> By repeating the x-ray measurements at varying times from the shock wave arrival, the density

throughout the dispersing particle curtain can be measured as it evolves in time. This is shown on the right side of Figure 4.

Over the last few years, the MST has provided both physical discovery and validation data for shock-induced particle dispersal. Such insight is critical to developing our predictive capabilities for explosive phenomena. Through advanced diagnostics and new experiments, the MST will continue to expand our knowledge base and enable accurate simulations of explosive events.

## References

- <sup>1</sup>S. Goroshin, D.L. Frost, J. Levine, S. Yoshinaka, and F. Zhang, "Optical Pyrometry of Fireballs of Metalized Explosives," *Propellants, Explosives, Pyrotechnics* 31, 3, 169-181, 2006.
- <sup>2</sup>F. Zhang, D.L. Frost, P.A. Thibault, and S.B. Murray, "Explosive Dispersal of Solid Particles," *Shock Waves* 10, 431-443, 2001.
- <sup>3</sup>J.L. Wagner, S.J. Beresh, S.P. Kearney, W.M. Trott, J.N. Castaneda, B.O. Pruet, and M.R. Baer, "A Multiphase Tube for Shock Wave Interactions with Dense Particle Fields," *Exp. Fluids* 52, 1507-1517, 2012.
- <sup>4</sup>G.S. Settles, *Schlieren and Shadowgraph Techniques*, Springer-Verlag, 2001.
- <sup>5</sup>Y. Ling, J.L. Wagner, S.J. Beresh, S.P. Kearney, and S. Balachandar, "Interaction of a Planar Shock with a Dense Particle Curtain," *Physics of Fluids* 24, 113301, 2012.
- <sup>6</sup>J.L. Wagner, S.P. Kearney, S.J. Beresh, B.O.M. Pruet, and E. Wright, "Flash X-Ray Measurements of Shock Wave Interactions with Dense Fields of Particles," *AIAA Paper* 2012-1054. ●

## The Los Alamos National Laboratory Turbulent Mixing Tunnel by Kathy Prestridge, John Charonko, and Nicolas Garcia (Los Alamos National Laboratory)

### Introduction

The Turbulent Mixing Tunnel (TMT) was commissioned at Los Alamos National Laboratory (LANL) to study variable-density turbulent mixing in subsonic flow conditions as a validation support facility for stockpile stewardship. Variable density mixing arises due to differences in molecular weights of mixing fluids or due to compressibility effects. Without the added complexity of shock waves moving about in the experiment, many measurements can be made in the TMT (see Figure 1) to establish statistical properties of the dynamic flow as a function of density variations and speeds. An open-circuit wind tunnel, the TMT draws ambient air into the tunnel inlet via an exhaust fan located downstream of the test section. The tunnel air exhausts to the outdoors. The tunnel dimensions are 0.5 x 0.5 x 5 m (from the inlet to the ground). Special care has been taken to control the flow inlet conditions using multiple screens and honeycombs.

### Variable-Density Turbulent Mixing and a New Approach

A detailed understanding of the mixing processes that occur in variable density turbulence is important for being able to accurately predict how fluids will mix in simulations. Two important examples of variable density turbulent mixing involve Rayleigh-Taylor and Richtmyer-Meshkov instabilities.<sup>1-4</sup> The comprehensive study of variable density turbulent mixing began in the 1980s at LANL with the pioneering theoretical works of Besnard and coworkers.<sup>5</sup> They developed a one-point transport model of variable density turbulence and important evolution equations for a number of second-order correlations of turbulent data. More recently, a second-moment closure model has been proposed<sup>6</sup> that describes turbulence quantities in flows with large density variations or fluctuations. The turbulence closures used are an extension of those proposed by Besnard et al.,<sup>5</sup> and they include closures for the turbulence mass flux and density-specific-volume correlation. These are important parameters that describe the energy within the variable-density mixing flow.

Unfortunately, there is not a complete understanding of the role of density variation in Richtmyer-Meshkov turbulent mixing—mostly due to the difficulty of taking measurements at the supersonic speeds and microsecond timescales that occur in these experiments. The **Extreme Fluids Team** in the Physics Division at LANL (see sidebar on page 10) made the first velocity field measurements<sup>7</sup> and the highest resolution measurements of shock-driven variable-density flows in the world.<sup>8</sup> The team is now leveraging their diagnostic capabilities to carefully measure important turbulence quantities in subsonic, variable-density flows.

In order to create variable-density mixing conditions in the TMT, a jet of dense sulfur hexafluoride gas ( $\text{SF}_6$ ) or air is seeded with acetone and small diethyl hexyl sebacate (DEHS) droplets and is injected into the test section of the tunnel. Figure 2 shows a cutout of the test section with the jet injecting into the center of the tunnel and the multiple diagnostic windows available for viewing the flow. The test section is equipped with a laser and optics to form a uniform light sheet (pictured in green) and cameras to measure the density and velocity as the jet mixes with the surrounding air. The flow diagnostics are the most sophisticated component of the experiment, by necessity. In order to measure the quantities needed to understand the turbulence in the flow, optical diagnostics are used. A pulsed Nd:YAG laser, producing 266 nm and 532 nm, illuminates the flow.

The density diagnostic, Planar Laser Induced Fluorescence (PLIF), uses the 266 nm light to make the acetone in the jet fluoresce at approximately 340 nm. This blue light is captured on a very sensitive digital camera, and a sample image is pictured in Figure 2a. By knowing the exact concentration of  $\text{SF}_6$  for a given fluorescence from gas analyzer measurements, that image can be translated into quantitative density field information in the imaging plane. The velocity diagnostic, Particle Image Velocimetry (PIV)<sup>9</sup> uses the 532 nm light to illuminate small particles that follow the flow over multiple pulses. One such particle image is pictured in Figure 2b. The particle displacements between two images are correlated to determine velocities, creating a snapshot of the two-dimensional (2D) velocity field.

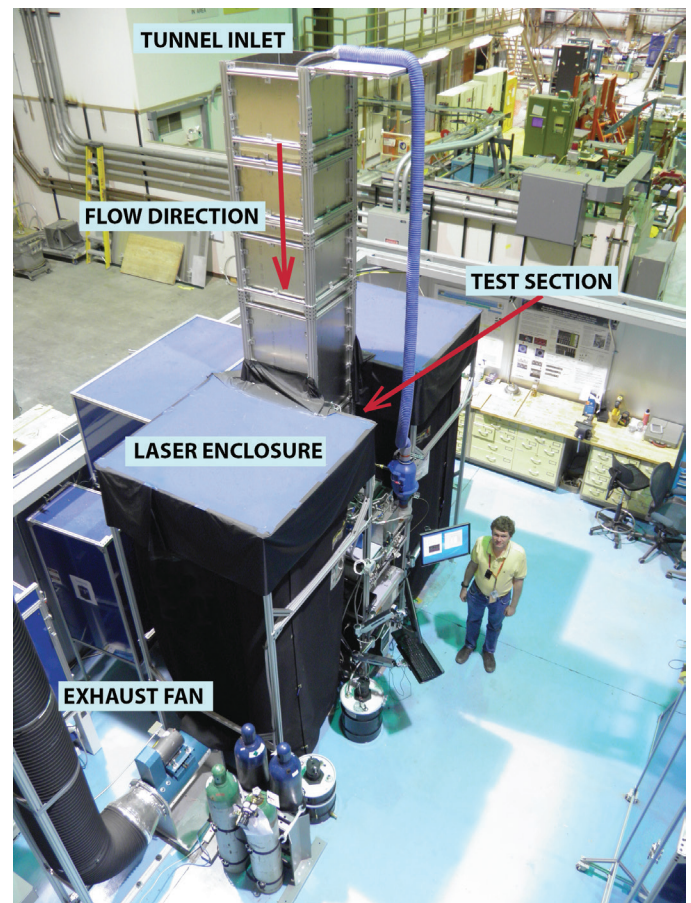


Figure 1. The Turbulent Mixing Tunnel is an open-circuit wind tunnel equipped with optical diagnostics to measure variable-density mixing phenomena for understanding and modeling variable-density turbulence.

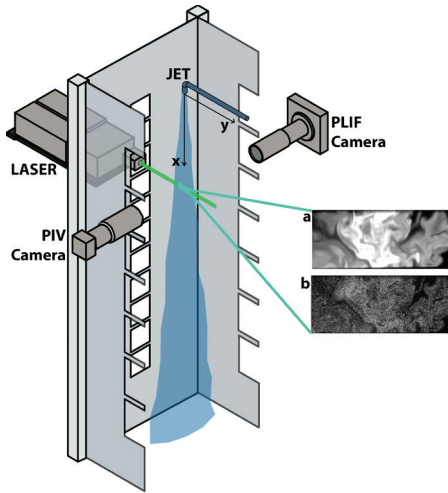


Figure 2. Cutout of the test section of the Turbulent Mixing Tunnel showing the jet, laser sheet, and two cameras for density (PLIF) and velocity field (PIV) measurements. Image (a) is a sample density field image, and (b) is one of a pair of particle fields used to calculate velocities.

### Statistical Turbulence Quantities and Measurements

The mixing that occurs in a variable density flow can be characterized through examination of the density fields, velocity fields, and correlations between those quantities. Figure 3 shows a density and velocity field for a high Reynolds number ( $Re=11,000$ ) air/acetone jet mixing with air. The Reynolds number is a measure of the momentum versus viscous forces in the flow, and a high Reynolds number represents a high-speed flow with small effects of viscosity. The measurement of density and velocity is in a plane 14.5 jet-diameters downstream from the jet exit, with spatial resolution of approximately  $100 \mu\text{m}$ . The experiment is run continuously, and many data sets such as the one in Figure 3 are taken. We use 2,000 to 3,000 datasets to calculate the average density and velocity fields, and from this, the fluctuations in the fields are then calculated. It is from these density and velocity fluctuations that turbulence quantities are derived.

One of those turbulence quantities, the Reynolds stress, determines how momentum is transported in turbulent, variable-density mixing flows. Reynolds stress is defined as follows:

$$R_{ij} = \overline{\rho' u_i' u_j'} - \overline{\rho} a_i a_j + \overline{\rho' u_i' u_j'}$$

$\rho$  is density,  $\mu$  the velocity, primes indicate fluctuating quantities, overbars

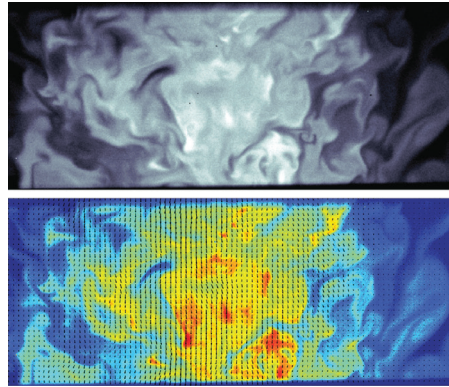


Figure 3. Upper image is of an air/acetone jet (white) mixing with pure air (black) at 14.5 diameters downstream from the jet exit. Flow is from top to bottom. Lower image is the density field, in false color, overlaid with vectors from the velocity field. The Reynolds number for this flow is 11,000.

indicate averages, and  $a$  is the turbulent mass flux velocity,  $a_i = \overline{\rho' u_i'} / \overline{\rho}$ . Subscripts are mathematical index notation, where  $i, j=1,2,3$ , and the numbers correspond to three spatial dimensions. This Reynolds stress has a more complex form than for constant density flows. In flows of constant density, the density fluctuations are zero, so the second and third terms are not present in typical flows. In order to measure the second and third terms of the Reynolds stress for variable-density flows, density and velocity must be measured simultaneously. Figure 4 shows the Reynolds stress profiles for three different experiments at two different locations, near the jet exit and farther downstream. By looking at these profiles, we can see that the higher density  $\text{SF}_6$  jet has much higher Reynolds stresses downstream than the air jet with the same initial volumetric flow rate. This is an effect caused by variable density, and this effect is something that we are continuing to quantify through more experiments at the TMT. Our experiments currently measure 2D velocity fields, but we will be expanding our capabilities in the future to measure the third velocity component using stereo imaging.

### Summary and Plans

The TMT is designed to be very sensitive to the effects of variable density on turbulent mixing through carefully controlled experimental conditions and high resolution measurements of density and velocity fields. The initial configuration of a single jet is being studied in more detail to gain a

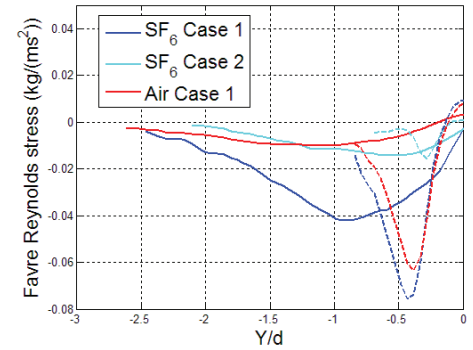


Figure 4. Reynolds stress profiles for three experimental jet cases in the near field (3 jet diameters downstream, dashed lines) and far field (14.5 jet diameters downstream, solid lines).  $y/d=0$  is the location of the jet centerline. The Air Case 1 and  $\text{SF}_6$  Case 1 start with the same Reynolds numbers, and the  $\text{SF}_6$  Case 2 is a lower Reynolds number. In the near field, the higher Reynolds number cases have higher turbulent kinetic energy, but further downstream, the air jet loses much more energy than the fast  $\text{SF}_6$  case.

### Extreme Fluids Team Physics Division Los Alamos National Laboratory

The Extreme Fluids Team is comprised of technical staff, postdoctoral research associates, and graduate and undergraduate students. As part of stockpile stewardship, the team works closely with the turbulence modeling, simulation, and validation efforts at LANL, such as the Computational Physics and Theoretical Design Divisions, to ensure that the experimental data are useful and relevant to modeling efforts. The team is part of the Center for Mixing Under Extreme Conditions, a joint national center comprised of Lawrence Livermore National Laboratory and LANL turbulence researchers. Additionally, all of the work for these experiments is published in peer-reviewed journals and presented at national and international conferences. More information about the team and its publications can be found at <http://www.lanl.gov/projects/shocktube/>.

better understanding of this spatially-evolving flow. The facility is capable of multiple configurations, and this year we will begin exploring those, including colliding heavy jets. The goal in the

next fiscal year is to develop a multi-jet array with a turbulence-generating grid that will create very uniform, or homogenous, velocity fluctuations in a variable density environment. There are many parameters that impact variable density flows, including the density, speed, and diffusion differences between the gases. In order to fully understand this problem, these variables must be studied and varied parametrically to determine the effects on turbulent mixing.

## References

<sup>1</sup>L. Rayleigh, "Investigation of the Equilibrium of an Incompressible Heavy Fluid of Variable Density," Proc. London Math. Soc. 14, 1884.

<sup>2</sup>G.I. Taylor, "The Instability of Liquid Surfaces When Accelerated in a Direction Perpendicular to Their Planes, I," Roy. Soc. London Proc. A. 201, 1950.

<sup>3</sup>R.D. Richtmyer, "Taylor Instability in Shock Acceleration of Compressible Fluids," Commun. Pure Appl. Math. 13, 1960.

<sup>4</sup>E.E. Meshkov, "Instability of the Interface of Two Gases Accelerated by a Shock Wave," Fluid Dyn. 4, 1969.

<sup>5</sup>D. Besnard, F.H. Harlow, R.M. Rauenzahn, and C. Zemach, "Spectral Transport Model for Turbulence," Theoretical and Comp. Fluid Dyn. 8, 1996.

<sup>6</sup>J.D. Schwarzkopf, D. Livescu, R.A. Gore, R.M. Rauenzahn, and J.R. Ristorcelli, "Application of a Second-Moment Closure Model to Mixing Processes Involving

Multicomponent Miscible Fluids," Journal of Turbulence 12, 2011.

<sup>7</sup>K.P. Prestridge, P.V. Vorobieff, P.M. Rightley, and R.F. Benjamin, "Validation of an Instability Growth Model Using Particle Image Velocimetry Measurements," Phys. Rev. Lett. 84, 19, 2000.

<sup>8</sup>K.P. Prestridge, G.C. Orlicz, S. Balasubramanian, and B.J. Balakumar, "Experiments of the Richtmyer-Meshkov Instability," Phil. Trans. Roy. Soc. A, 371, 2013.

<sup>9</sup>R.J. Adrian and J. Westerweel, Particle Image Velocimetry, Cambridge University Press, Cambridge, 2011. •

## Precision Calculations for Circuits in Hostile Environments by C.E. Hembree and E.R. Keiter (Sandia National Laboratories)

Sensing and calculating electronic systems with stringent accuracy requirements use internal standard voltages for references. Conceptually, this is related to using some unit measurement for counting any quantity. The high precision electronic components used in systems in the nation's stockpile also make use of these standard voltages.

The need for stable voltage references has been long-standing in the overall electronics industry. For many applications, the most pressing need is for stability of a reference voltage as the circuit temperature varies. Typical circuit components have temperature coefficients for their operational characteristics that are given in some delta per degree centigrade, and these coefficients can be either positive or negative. Therefore, it is natural to consider building a circuit out of components that have complementary temperature coefficients so that the operating characteristics of the circuit have a net zero temperature coefficient. This is the fundamental basis of precision voltage reference (PVR) circuit operation and it is straightforward to extend this type of stabilization to reduce shifts caused by hostile environment radiation.

In some stockpile applications, the requirements for stability of the voltage

reference ( $V_{ref}$ ) are unusually demanding for analog electronic components. These requirements make this class of circuits interesting to study with simulations to illuminate the mechanisms that provide challenge to the stability of  $V_{ref}$ . The topology of these circuits compound the challenge since the PVR circuit is coupled to a separate amplifier that is often built with a different semiconductor technology. Modeling such an amplifier in hostile environments can mean that additional radiation physics models are required.

Hostile environment simulations of PVR circuits are underway at Sandia National Laboratories (SNL) with funding from the Nuclear Survivability Engineering Campaign and the Advanced Simulation and Computing (ASC) Program. The simulations generate information to be used in design and qualification of systems using these circuits. This report describes the operation of a generic PVR circuit and the challenges involved with these simulations.

In order to study the abilities of this circuit to cope with fluctuations, it is necessary to understand how the circuit design maintains a constant  $V_{ref}$ . This type of circuit is a Brokaw circuit<sup>1</sup> which is a type of stabilized band gap voltage circuit. The design of the circuit is optimized for stability under temperature excursions<sup>2</sup> and is

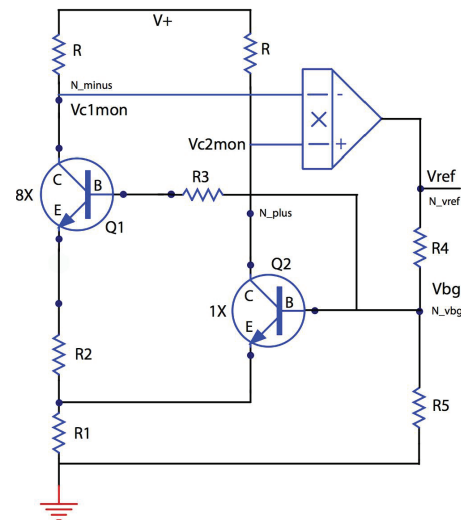


Figure 1. A simplified schematic of the Brokaw-based band gap reference circuit. Currents in the two transistors  $Q1$  and  $Q2$  are forced to be equal by the external op-amp.  $V_{bg}$  is the generated band gap output voltage and  $V_{ref}$  is the higher-by-design reference output voltage.

based on transistor characteristics well-behaved with temperature.<sup>3</sup> The circuit is modified with an additional resistor to provide stability against radiation-induced changes. Figure 1 displays a schematic of a PVR circuit.

The principle components of a band gap circuit are two current paths incorporating resistors so that two

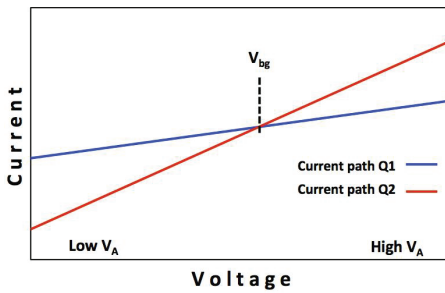


Figure 2. Two currents flowing in two current paths in a hypothetical bandgap circuit.

current dependent voltages are generated. The two current paths also include circuit elements such as diodes or transistors that control the current as a function of applied voltage ( $V_A$ ). Refer to Figure 2 to view a graph representing these currents.

The two current paths are designed so that the two controlling circuit elements regulate the currents in each path at different rates with respect to the controlling voltage. In addition, these circuit elements are designed to provide different currents at some initial low  $V_A$ . In this way, one of the circuit elements (i.e.,  $Q1$ ) with a higher initial current at low voltages can be constrained to increase its current with applied voltage at a slower rate than the other circuit element (i.e.,  $Q2$ ).  $Q2$  has a lower initial current at low applied voltages and a faster rate of current increase with applied voltage. It can be forced to pass an identical current as  $Q1$  at some applied voltage. As the applied voltage is increased from low to high, the two current paths start with unequal currents that converge at some applied voltage and then diverge as the applied voltage is further increased.

The currents through  $Q1$  and  $Q2$  are monitored by the generated voltages at the resistors in the current paths. The behavior of these monitor voltages ( $VC1_{mon}$  corresponds to  $Q1$  and  $VC2_{mon}$  corresponds to  $Q2$ ) is similar to the currents as a function of the applied controlling voltage. At the applied voltage (call it  $V_{bg}$ ) where the currents are equal,  $VC1_{mon} = VC2_{mon}$ . At all other values of the controlling voltage, the monitor voltages are unequal and  $VC1 < VC2$  for  $V_A < V_{bg}$  and  $VC1 > VC2$  for  $V_A > V_{bg}$ . This polarity reversal at  $V_{bg}$  is sensed by an operational amplifier and used to control the band gap circuit

by influencing the applied voltage to the circuit elements  $Q1$  and  $Q2$ . This operational amplifier can be configured so that the net applied voltage is forced to the  $V_{bg}$  voltage where the currents are equal.  $V_{bg}$  is related to the circuit precision output voltage  $V_{ref}$  through a resistor.

The challenge of modeling this circuit setup in radiation environments is to model the normal operation of the circuit to 1% error or less (including temperature effects) and also the effects of radiation on the transistors ( $Q1$ ,  $Q2$ ) within the PVR circuit as well as radiation effects to the operational amplifier. Ongoing work at SNL using an ASC simulation code known as Xyce is directed towards constructing high accuracy simulations of the transistors that include transistor physical degradations arising from displacement damage caused by neutron or heavy ion radiation.

The displacement damage radiation effects reduce the  $Q1$  and  $Q2$  currents but not equally. In this way, the intersecting voltage where the currents are equal varies slightly and this variation leads to instabilities in the output  $V_{ref}$  voltage since  $V_{ref}$  is related to  $V_{bg}$ . The radiation modeling of this circuit effect must account for different radiation responses between  $Q1$  and  $Q2$  that may vary stochastically. This stochastic response is due to the radiation-caused generation of defects and may be non-uniform in small devices. The radiation response calculations are based on computations of defect-induced recombination currents and increases in device resistivities as a function of defect densities.

In typical simulations, the radiation responses of the  $Q1$  and  $Q2$  transistors are varied independently to reflect the experimentally known result that neutron damage in small transistors is variable. This leads to  $V_{ref}$  shifts to both higher and lower voltages than the pre radiation voltage. It is of interest to model these effects in an ensemble of circuits rather than individual circuits so uncertainties are included for the phenomena being simulated. This treatment of the damage uncertainty yields a distribution of shifts that can be compared to similar distributions compiled from experiment.

The Xyce code also includes models to replicate the additional charge introduced in some transistors by ionizing radiation. This dose rate dependent radiation model utilizes device geometry information to calculate total generated charge. This charge results in voltage offsets within the operational amplifier associated with photo-currents and also causes time-dependent current surges between the PVR and the operational amplifier.

These voltage offsets are transient and depend on the configuration of devices in the operational amplifier circuit. These in turn will influence the operational amplifier output voltage and this affects the controlling voltage of the PVR. These transient effects introduce further variation into the value of  $V_{bg}$  and thus  $V_{ref}$ .

Although the PVR simulations are still under refinement, the results to date indicate good fidelity with measured data of these circuits in radiation environments. More work is planned to further develop the physical degradation models and to complete the calculations with relevant uncertainties that will enable a calculation of circuit performance margin with respect to requirements.

## References

- <sup>1</sup>A.P. Brokaw, "A Simple Three-Terminal IC Bandgap Reference," IEEE Journal of Solid-State Circuits, SC-9(6):388-393, December 1974.
- <sup>2</sup>R.J. Widlar, "New Developments in IC Voltage Regulators," IEEE Journal of Solid-State Circuits, SC-6(1):2-7, February 1971.
- <sup>3</sup>J.S. Brugler, "Silicon Transistor Biasing for Linear Collector Current Temperature Dependence," IEEE Journal of Solid-State Circuits, SC-2(1):57-58, June 1967. •

## Contact Us

Please send your comments about this issue of the *Stockpile Stewardship Quarterly* and suggestions for future issues to Terri Stone at [terri.stone@nnsa.doe.gov](mailto:terri.stone@nnsa.doe.gov). To subscribe to our mailing list, submit your full name, email address, and organization.

